Avalon Campus
1 Fairway Drive
Lower Hutt 5011
PO Box 30368
Lower Hutt 5040
New Zealand
T +64 4 570 1444
www.gns.cri.nz

Consultancy Report 2025/40 LR
Project No: COMN0338

16 April 2025

Christchurch City Council
PO Box 73016
Christchurch 8154

Co-seismic and post-seismic rates of vertical land movement in the Canterbury Region and implications for future changes in sea level

1.0 Introduction

In 2022, the New Zealand SeaRise programme released new probabilistic relative sea-level projections, including the different Shared Socioeconomic Pathways (SSP) scenarios, using the Framework for Assessing Changes to Sea-level (FACTS) from the Intergovernmental Panel on Climate Change (IPCC) Assessment Report 6 (Fox-Kemper et al. 2021; Garner et al. 2021). Notably, this approach incorporated a novel component to incorporate local vertical-land-movement data (Kopp et al. 2023). These projections were generated at 2 km intervals along New Zealand's coast (Naish et al. 2024).

To minimise the potential temporal biases introduced by local earthquakes in future projections of vertical land movement, estimates were derived from historic Envisat Synthetic Aperture Radar (SAR) data acquired between 2003 and 2011 (Hamling et al. 2022). This period largely preceded many of the magnitude 6 or greater earthquakes that have struck New Zealand since late 2009, making it a more representative sample of inter-seismic vertical land movement. However, large earthquakes across Canterbury have resulted in accelerated rates of uplift (such as the 2016 Kaikōura earthquake) and drastically increased rates of land subsidence in areas such as eastern Christchurch. Given that patterns of post-earthquake vertical land movement are likely to continue for some time, it is worth considering the implication for future projections of local relative sea-level rise across the Christchurch district. In 2023, Christchurch City Council (CCC) and Environment Canterbury (ECan) jointly commissioned a report examining the influence of co- and post-seismic deformation across the Christchurch district. The analysis was based on Sentinel-1 SAR data from a single frame from April 2015 to July 2022 generated as part of a PhD project at the Victoria University of Wellington (Hamling and Kearse 2023a, 2023b). The aim of this report is to extend the analysis of Hamling and Kearse (2023a) to encompass the wider Canterbury region (Figure 2.1), increase the length of the time series of Senetinel-1 data being used up to October 2024 and take advantage of the additional satellite frames now available. After discussions with CCC and ECan, an area of interest was selected that encompasses the entire Christchurch district, as well as several coastal areas (and up to ~20 km inland) of the Kaikōura, Hurunui, Waimakariri, Selwyn, Ashburton and Timaru districts.

2.0 Co-Seismic Deformation Estimates

In countries that sit along active plate margins, such as New Zealand, there is a need to consider both the instantaneous vertical land movement caused by earthquakes as well as the long-term movement of the Earth's surface between them. While we cannot predict if and when a given stretch of coastline will experience a future earthquake, incorporating the vertical land movement from known past earthquakes allows us to update estimates of local sea-level rise and provide a mechanism to evaluate and stress-test future scenarios. To estimate the amount of ground movement caused by the earthquakes, we use fault-slip models. These models use observations of how the ground moved during an earthquake to provide an estimate of how much a fault moved (slipped) and predict how much the ground moved in areas where we may not have observations. Here, we estimate the net co-seismic offsets caused by the 2010/11 Canterbury Earthquake Sequence and 2016 Valentine's Day (Christchurch) and 2016 Kaikōura earthquakes using a combination of published and unpublished slip models (Table 2.1; Figure 2.1). In addition, due to the large observed post-seismic deformation in and around Kaikōura following the 2016 event, we include the six-month afterslip models of Wallace et al. (2018). Due to their smaller magnitudes and faulting mechanisms, there was likely negligible post-seismic deformation associated with the other earthquakes and so only their co-seismic deformation is included.

Table 2.1 List of earthquakes affecting the area of interest shown in Figure 2.1 and source of models used to estimate the total vertical offsets. InSAR = Interferometric Synthetic Aperture Radar.

Earthquake(s)	Model Source
2010/11 Canterbury Earthquake Sequence	Beavan et al. (2012)
2016 Valentine's Day earthquake (Christchurch)	Unpublished inversion of InSAR data
2016 Kaikōura earthquake	Hamling et al. (2017)

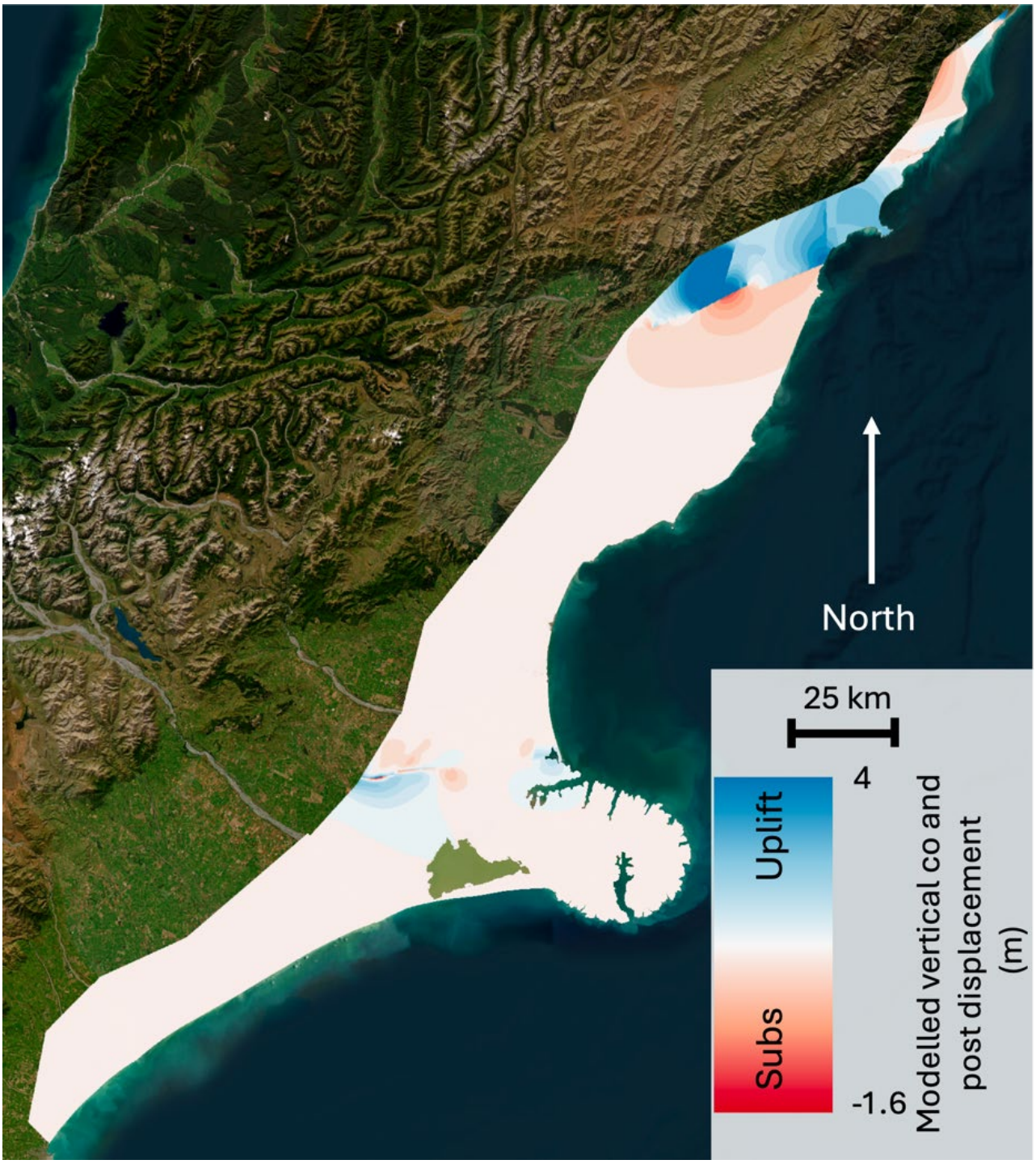

Figure 2.1 Total vertical displacement calculated from co-seismic slip models for the 2010/11 Canterbury Earthquake Sequence, 2016 Valentine's Day earthquake (Christchurch) and 2016 Kaikōura earthquake. The vertical displacement also includes the first six months of post-seismic deformation following the Kaikōura earthquake (Wallace et al. 2018).

While the co-seismic models provide an estimate of the vertical deformation resulting from fault movement, these do not provide information on secondary processes such as lateral spreading and liquefaction. For the Christchurch district, where liquefaction was widely observed, we follow the earlier approach of Hamling and Kearse (2023a, 2023b) and use the LiDAR (Light Detecting and Ranging) difference model (Hughes et al. 2015; Figure 2.2) as a direct measure of the co-seismic offset. In regions without LiDAR coverage, we rely on the modelled vertical deformation derived from the co-seismic slip models outlined above. Similarly, in the Kaikōura district, most notably around the Clarence River, co-seismic models do not readily capture the true extent of the vertical deformation attributed to the Papatea Fault during the earthquake (Langridge et al. 2018; Diederichs et al. 2019; Figure 2.2b). While traditional kinematic models used to estimate ground deformation from the 2016 Kaikōura earthquake successfully estimated the regional-scale ground deformation, these struggled to explain the faulting along the Papatea Fault; notably, the extremely large uplift the to the west of the Clarence River. To better capture the uplift, we use the vertical deformation estimated from SAR offset data (Hamling et al. 2017; Figure 2.2b).

The most significant co-seismic deformation is found in the Kaikōura and Hurunui districts as a result of the 2016 Kaikōura earthquake. Areas immediately west of Clarence River were uplifted by up to 8–10 m (Hamling et al. 2017; Hamling 2020), with inland areas also experiencing metres of uplift in some areas. From Hundalee and to the south, the Kaikōura earthquake resulted in subsidence of ~0.5 m near Hundalee, decreasing to 30–40 mm towards the Waimakariri and Christchurch districts. For these districts, the more significant co-seismic deformation came from the earlier 2010/11 Canterbury Earthquake Sequence. As reported by Hamling and Kearse (2023a), kinematic slip models, which do not account for processes such as liquefaction or shaking-related settlement, predict uplift of ~400 mm around New Brighton and the Heathcote and Avon Estuary. North of New Brighton, co-seismic subsidence dominates, with ~130 mm predicted north of Waimairi Beach. However, as noted earlier, liquefaction caused significant local ground deformation exceeding 1 m in some areas (Hughes et al. 2015; Figure 2.2). Differential LIDAR observations from before and after the earthquake sequence (Hughes et al. 2015; Figure 2.2) show much of the New Brighton / Southshore coastline locally subsided by ~100–200 mm, indicating that the localised subsidence from liquefaction was larger than the uplift caused by faulting.

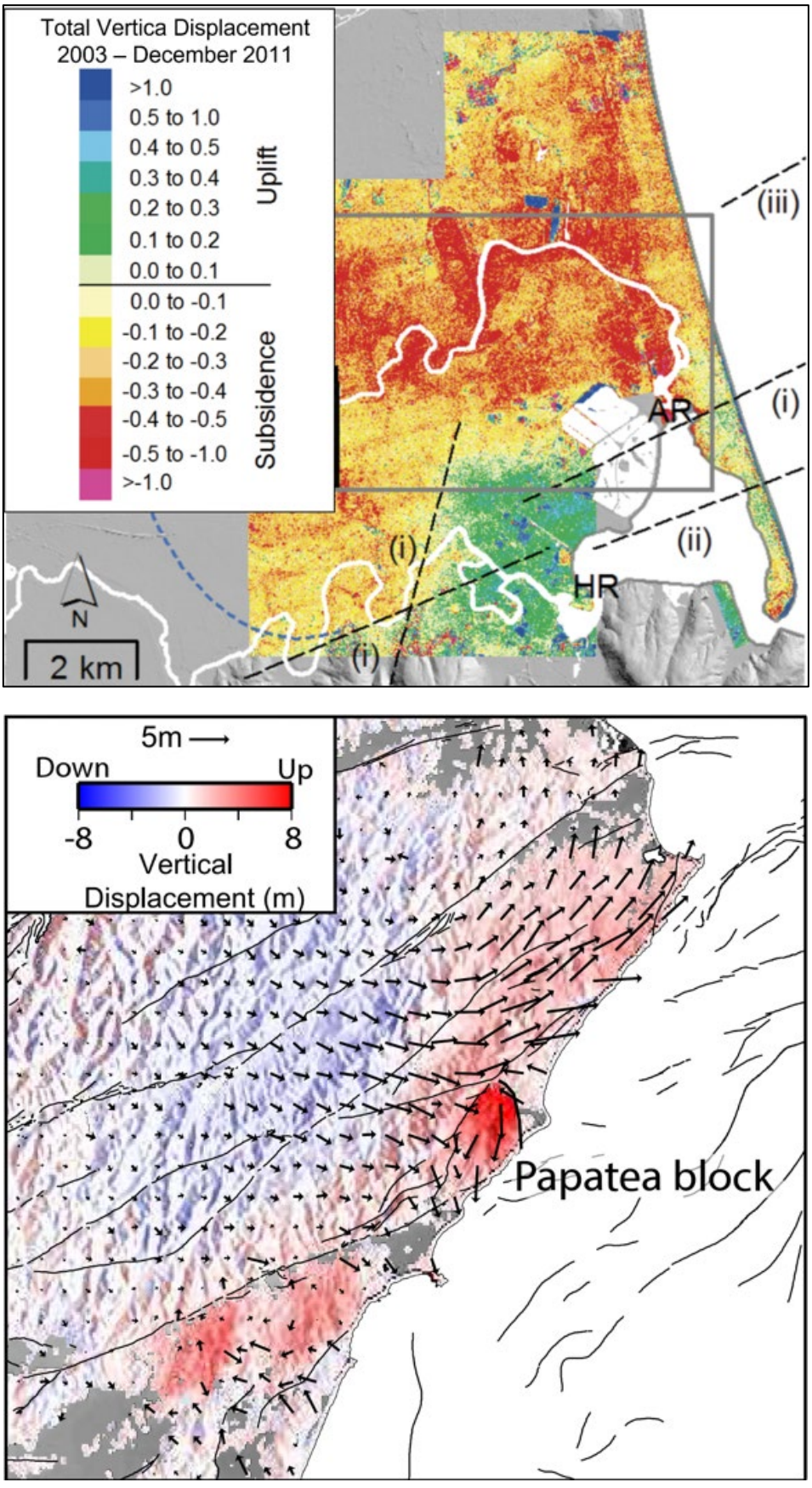

Figure 2.2 (Top) Total vertical displacement derived from differential LiDAR surveys in 2003 and December 2011. Figure modified from Hughes et al. (2015). (Bottom) Three-dimensional displacement field from the Kaikōura earthquake derived from SAR azimuth and range offsets (Hamling et al. 2017). Arrows show the horizontal movement; the coloured background is the vertical displacement.

3.0 InSAR Dataset and Revised Vertical-Land-Movement Estimate

Interferometric Synthetic Aperture Radar (InSAR) is a monitoring technique that uses radar imagery to measure ground movement. SAR images are usually acquired using satellites, aircraft or unmanned aerial vehicles (UAVs), and the phase component of their emitted signal is differenced to produce a map of ground deformation called an interferogram. A single interferogram is capable of measuring the ground displacements associated with significant events, such as earthquakes, volcanic unrest or landslides. However, to accurately measure slow, steady movements on the order of millimetres per year, we need to combine many interferograms to produce a time history of ground movement.

The data provided here has been processed using Sentinel-1 (a satellite operated by the European Space Agency) SAR data by SatSense Ltd. They specialise in processing InSAR data with a proprietary software called RapidSAR (Spaans and Hooper 2016). RapidSAR follows a standard industry-recognised processing chain, rigorously identifying points on the ground surface that consistently provide stable reflections of the SAR signal. Their approach enables the analysis of persistent scatterers (PS; i.e. point-based coherent target evaluation) and distributed scatterers (DS; i.e. area-based target evaluation) in a common processing chain to achieve the highest possible point density.

To derive the estimated vertical land movement across Canterbury, we collate and extract all of the available InSAR data covering the region from both ascending (satellite flying south to north) and descending (satellite flying north to south) orbit geometries. The timespan of the data varies depending on the satellite pass. The earliest acquisition was in May 2015 and the latest in October 2024, with maximum coverage from after the Kaikōura earthquake. The data is first quality-controlled using the average coherence and Root Mean Square Error (RMSE) of each point to reduce the number of unreliable scatterers. Using the full time series, we then solve for the best-fitting linear velocity for each point, including sinusoid with annual components.

Unlike Global Navigation Satellite Systems (GNSS), which measure the three components (east–west, north–south and up–down) of ground displacement in an absolute reference frame, InSAR provides only a relative 1D line-of-sight (LOS) measurement (Figure 3.1). Furthermore, because of the near north–south flight path of the satellite, InSAR is insensitive to movement in that direction (north–south). If both ascending and descending data are available, and we have GNSS to help constrain the north–south motion, InSAR can be deconvolved into the east–west and vertical components. However, the derived displacement is still only a relative measure. Hamling and Kearse (2023a, 2023b) used the regional GNSS data across the Christchurch district (provided by Paul Denys at the University of Otago and the national GNSS network) to help tie the InSAR-estimated vertical land movement into the same reference frame as the GNSS (ITRF2014). Here, we use a different approach. To be consistent with ongoing work on a revised national vertical-land-movement dataset, we use the nationwide GNSS data to provide the tie rather than just the local network. This has the advantage of incorporating the larger spatial component of tectonic movement that would be missed when using only local observations for the tie. For each GNSS site, we use the time series computed by the Nevada Geodetic Lab (Blewitt et al. 2018) and re-estimate the annual velocity using data from after the Kaikōura earthquake. To limit the potential bias of the large post-seismic deformation being propagated into vertical-land-movement rates and future sea-level rise projections, we trim the time series at stations north of Hundalee to contain only data after the rates of post-seismic deformation had stabilised in 2020. Using these velocities, we interpolate the GNSS station velocities onto the same grid as the InSAR, following the method of Wang and Wright (2012) (Figure 3.2). For each InSAR dataset, we project the interpolated GNSS data into the satellites LOS direction and estimate the residual difference between their velocities. We then fit a third-order polynomial ramp through the residual field and subtract it from the InSAR data, placing the InSAR in the same reference frame as the GNSS (Watson et al. 2024; Figure 3.1).

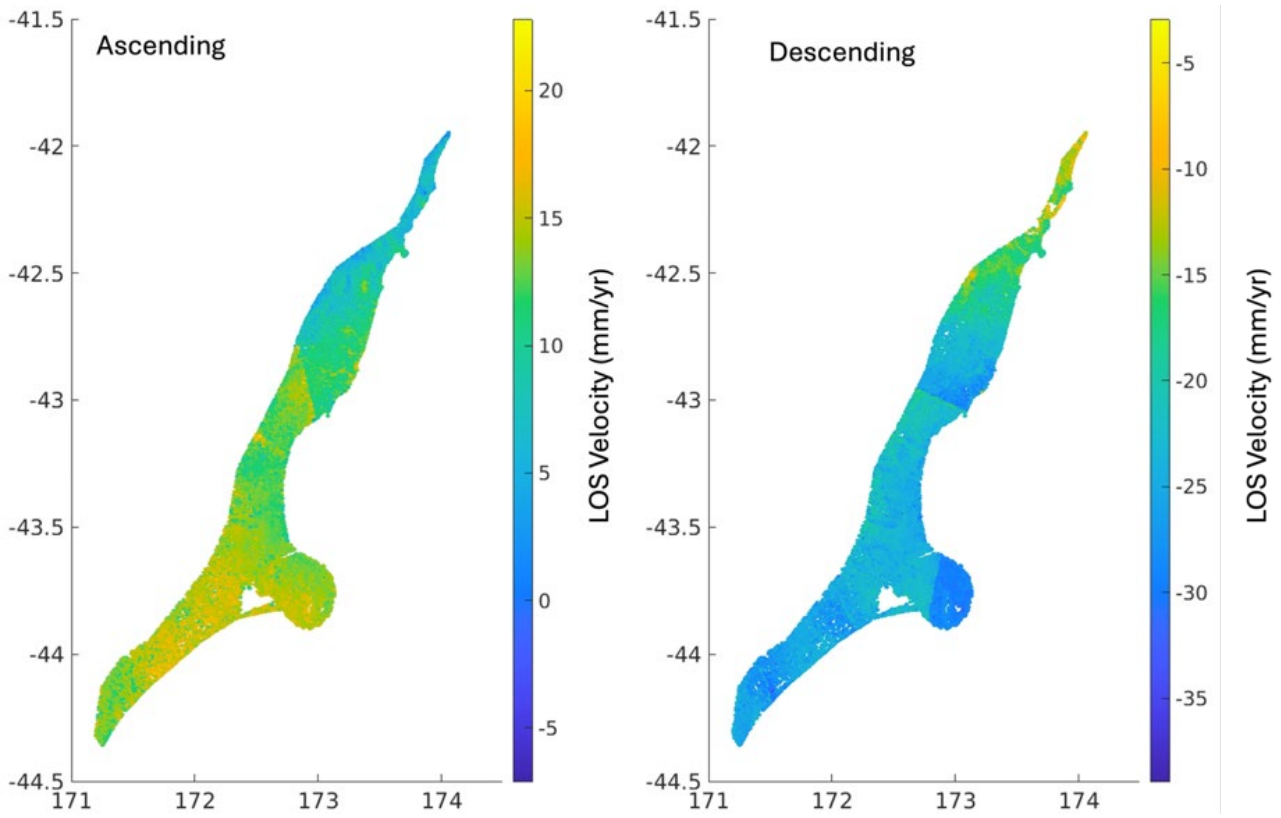

Figure 3.1 Combined ascending and descending LOS velocities after tying to the GNSS. Linear discontinuities show the location of SAR frame boundaries and associated changes in the look angle.

After tying the InSAR into the GNSS reference frame, we generate a uniformly spaced grid to estimate the 3D displacement field. Due to the higher data density within the Christchurch district, the grid spacing is set to 50 m with the remainder of the regions sampled at 100 m. In a final step, using the ascending and descending InSAR datasets and the interpolated GNSS velocity fields, we solve for the three components of the velocity (Figure 3.2). Observations are weighted by their individual uncertainties, and we apply an additional weight to the InSAR data based on the land-cover class to reduce the impacts of any phase bias (Ansari et al. 2021) such that points located on urban or bare ground, which are typically more stable reflectors, are weighted more highly than points on agricultural land or forest. Uncertainties are estimated by perturbing each observation 500 times by adding or subtracting their scaled uncertainty and calculating the mean and standard deviation. Although efforts to remove the phase-bias are largely successful, some areas still show an apparent bias. This is most notable in the northern areas where many of the braided river channels show a relative uplift compared with the surrounding ground. Although a component of this may be related to aggradation within the channel bed, the consistency of the signal across multiple rivers suggests some residual phase bias may still be present.

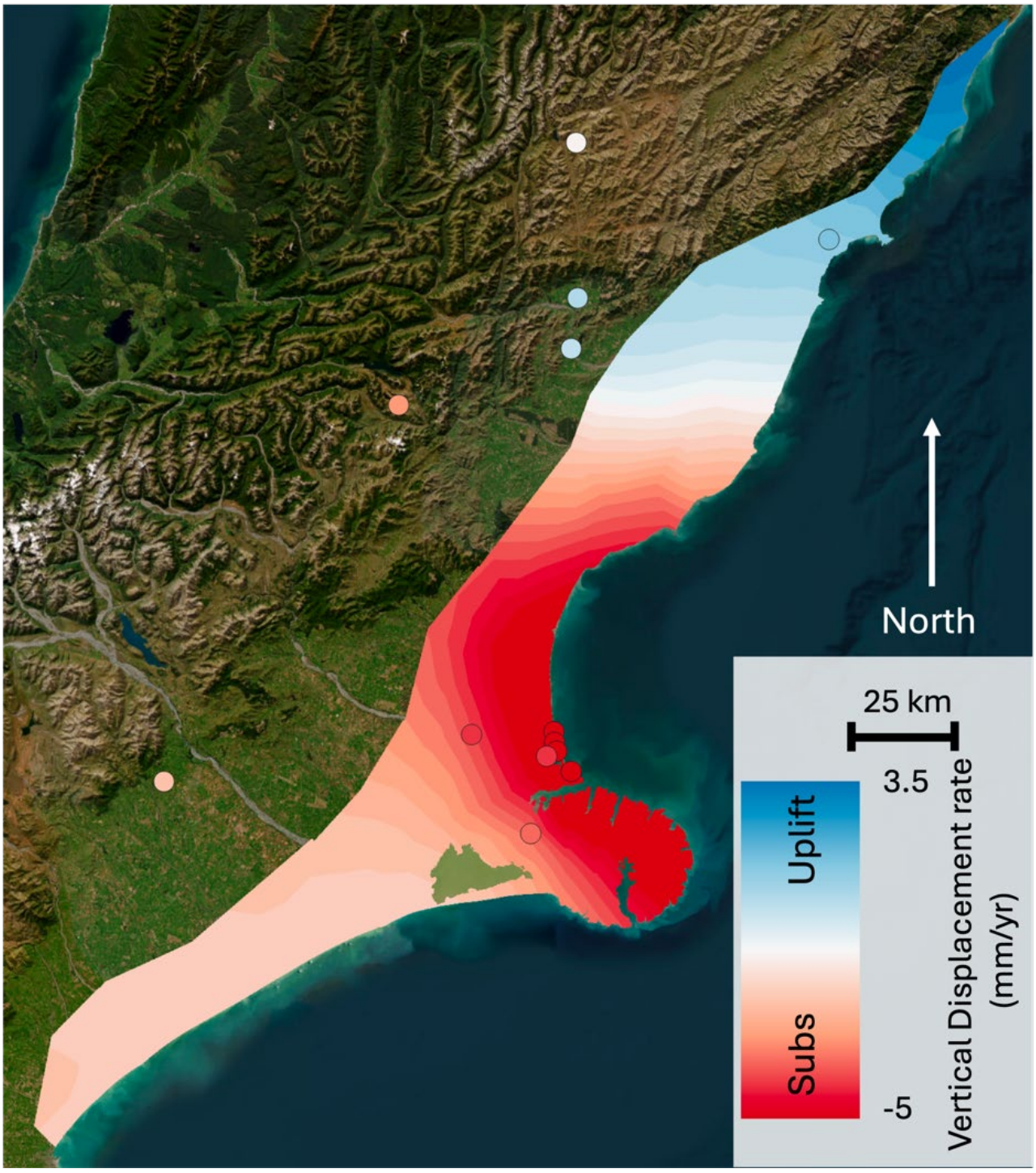

Figure 3.2 Estimated long-wavelength component of the vertical velocity field. The coloured dots show the observed vertical rates at GNSS stations.

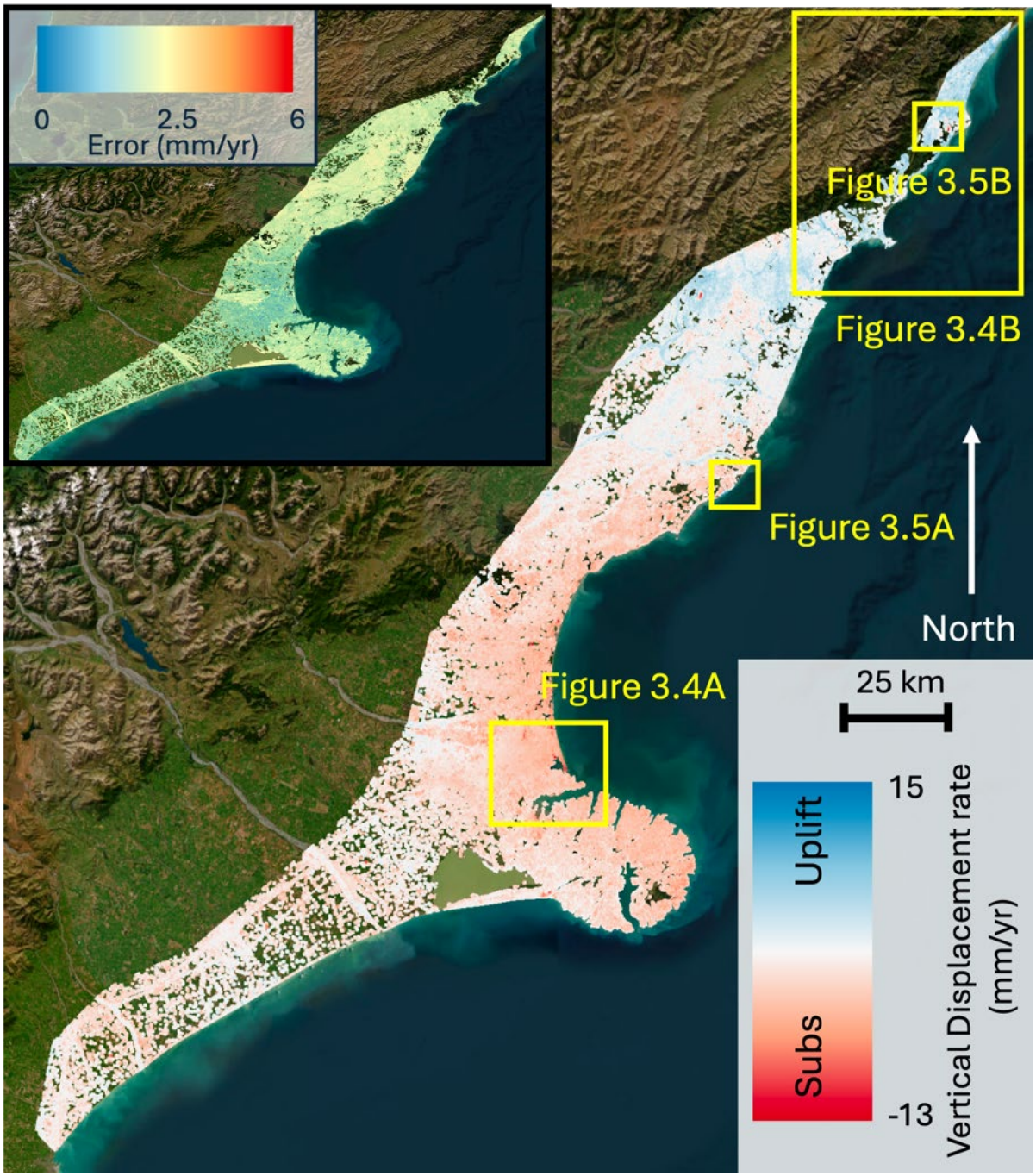

Figure 3.3 Estimated vertical component of the velocity fields calculated from the combined InSAR and GNSS datasets. Yellow boxes show the locations of subsequent figures and the map in the top left shows the estimated uncertainty associated with the vertical rate estimates.

In the final dataset (Figure 3.3), both the tied InSAR and interpolated long-wavelength GNSS vertical rates (Figures 3.2 and 3.3) are included. The long-wavelength component provides an estimate of the regional vertical land movement being driven from large-scale processes (i.e. tectonics) but does not capture additional vertical land movement from more localised sources such as landslides or compaction. Across the whole region, there is a general pattern of uplift in the north (Kaikōura and Hurunui districts; Figure 3.3) because of the ongoing post-seismic deformation from the 2016 Kaikōura earthquake, with subsidence south of the Waiau Uwha river around Christchurch City (Figure 3.4a) and Banks peninsula. While north of Half Moon Bay in Kaikōura District there is net uplift (Figure 3.4b), large coastal landslides above the state highway and inland cause localised zones of relative subsidence (Figure 3.5b). In contrast, south of Napenape, large rotational landslides lead to localised uplift along the coast (Figure 3.5a).

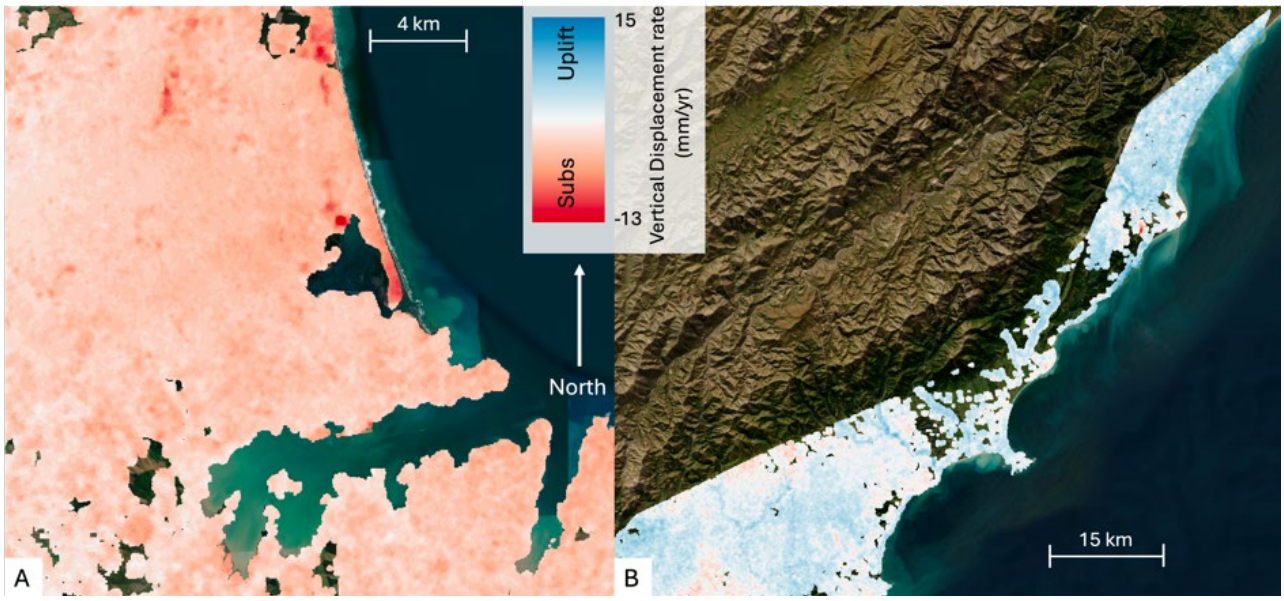

Figure 3.4 Differences in vertical displacements focused around (a) Christchurch and (b) Kaikōura.

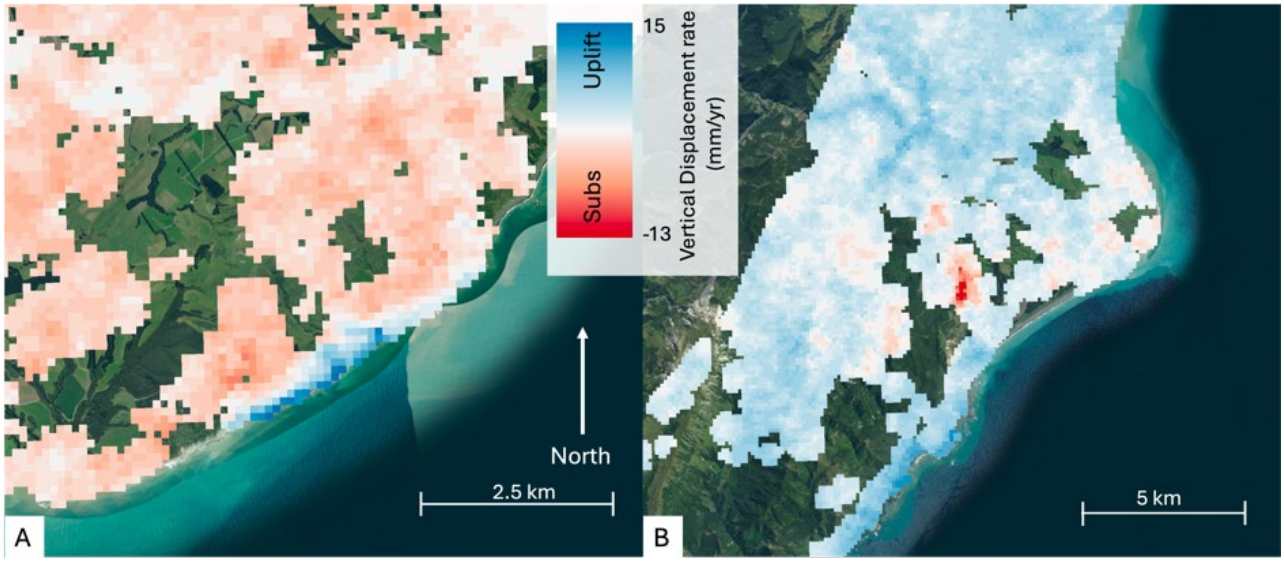

Figure 3.5 Differences in vertical displacements associated with coastal landslides near (a) Napenape and (b) the Clarence river mouth.

Based on the GNSS data, the highest subsidence rates are within the Christchurch City area where data from the University of Otago (Pearson and Denys 2024) shows rates of ~4 mm/yr (Figure 3.2). Outside of the city, the national GNSS network has slightly lower rates of subsidence of 2–3 mm/yr. In the combined dataset, which captures both the regional and local vertical land movement, the addition of the InSAR highlights several zones of focused subsidence within Christchurch. In addition to the higher rates previously noted across New Brighton (7–12 mm/yr), there are also elevated rates of subsidence (>5 mm/yr) around the Bromley industrial area, Lyttleton Port and Sumner. In Lyttleton Port, subsidence is focused on areas of reclaimed land, with heavy infrastructure around Charlotte Jane Quay. In Sumner, localised subsidence is found extending from Colenso Street towards the promenade in areas built on Holocene beach deposits. Other localised areas of subsidence are in areas of recent construction, such as around the Parakiore Recreation and Sport Centre, and may be related to post-construction compaction.

4.0 Revised 2 km Vertical Land Movement and Relative Sea-Level Rise Projections

To generate the revised relative sea-level rise projections, we follow a similar approach as detailed in the report by Hamling and Kearse (2023a) and its addendum (Hamling and Kearse 2023b). Co-seismic and post-seismic deformation (Kaikōura only) for coastal sites are made up from a combination of co-seismic models, differential LiDAR and SAR offsets (Table 2.1; Figure 2.1). For each 2 km coastal site, Hamling and Kearse (2023a) used an inverse distance-weighting for the spatial averaging. Here, we search for all InSAR points within 250 m and take the distance-weighted average using an exponential weight function (Figure 4.1). Although the net effect is similar, by including an exponential term, nearby points get even higher weights. Points located on bare ground or in urban areas are also given higher weights to limit the effect of any residual phase bias still present in the data. If there are less than 20, we incrementally increase the search radius by 250 m, avoiding taking samples across water bodies, up to a maximum of 5 km until 20 points are found. Because of the increased spatial coverage of the dataset, 95% of the samples are within 750 m.

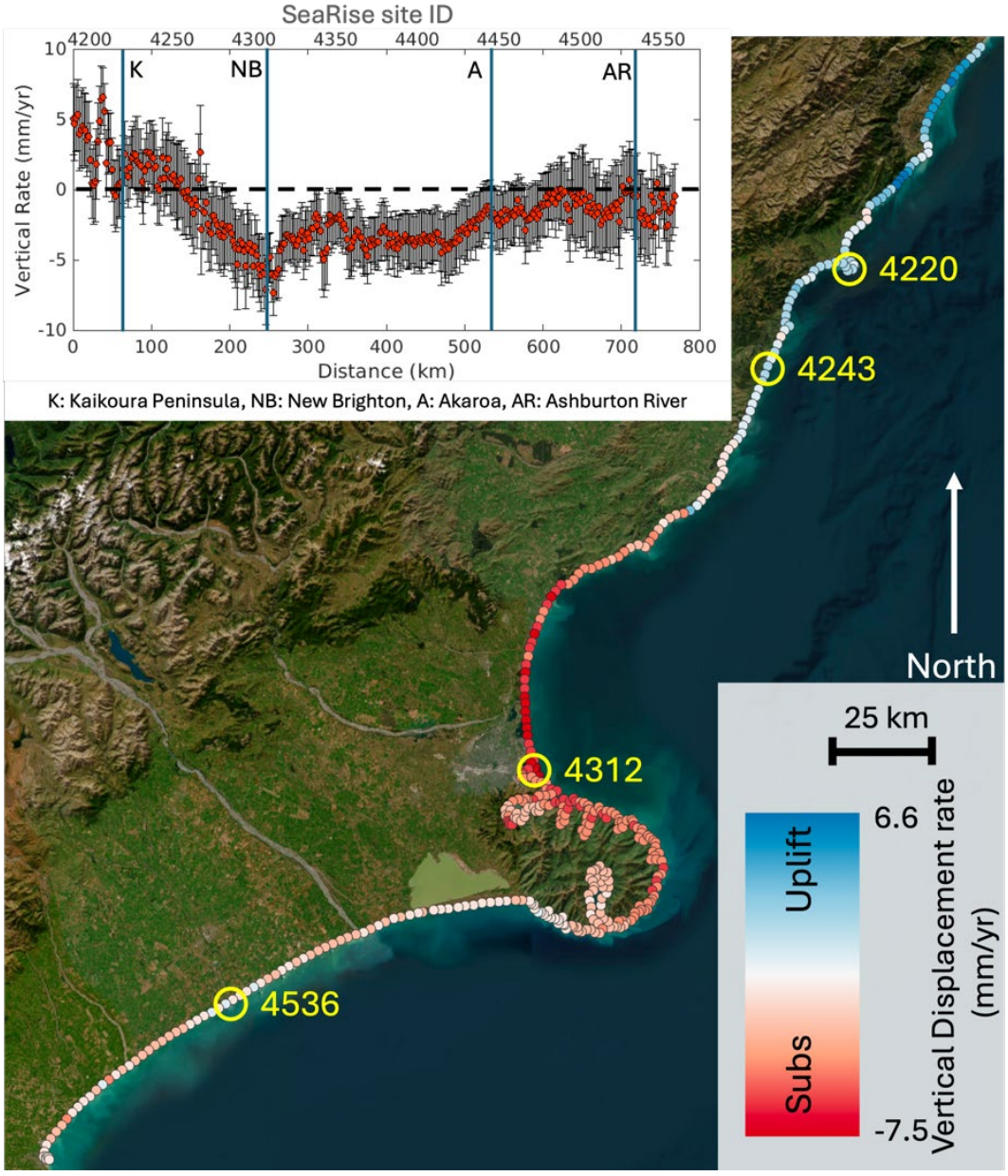

Figure 4.1 Re-estimated vertical-land-movement rates binned at 2 km intervals. The inset in the top left shows a profile through all of the coastal sites from north to south.

To calculate the relative sea-level rise projections, we first remove the vertical-land-movement contribution based on the inter-seismic rates determined by Hamling et al. (2022) and Naish et al. (2024). Increased post-seismic velocities are commonly observed following moderate to large earthquakes (Ingleby and Wright 2017). Variations in geology can have a significant effect at a local scale, but global compilations suggest that post-earthquake velocities decay at a rate of 1/t, where 't' is the time since the earthquake in years (Ingleby and Wright 2017), and may return to inter-seismic rates within decades (Hussain et al. 2018). For the Kaikōura earthquake, while not back to pre-event vertical rates (~-1 to -3 mm/yr), the GNSS at Cape Campbell measured ~300 mm of additional uplift up until 2020, most of which occurred in the first 12 months. Since then, uplift has continued but only accumulated an additional 40 mm, and the rate continues to decrease as the post-seismic stresses relax. In contrast, areas around New Brighton in Christchurch continue to show higher rates of subsidence that have persisted for the last ~10 years, as supported by local GNSS data from the University of Otago.

To explore the effects of post-seismic transients persisting for different amounts of time, we apply the newly estimated vertical-land-movement rates out to 2030, 2050, 2100 and 2150. At those times, the vertical-land-movement rates return to the inter-seismic rates published by NZ SeaRise. Considering the observed temporal evolution of the post-seismic deformation around Kaikōura and decaying uplift rates, the most likely scenario is that rates will return to close to their inter-seismic rates by 2030 or 2050. However, allowing for increased rates out to 2100 in areas where the driving mechanism behind the localised subsidence is likely different, such as New Brighton, provides a likely worst-case scenario to test against. For the examples below, we use the SSP2-4.5 medium confidence projections provided through the Takiwa portal (https://searise.takiwa.co/). The selected examples are chosen to cover the range of different vertical-land-movement rates from across the region. In all figures, the black lines show the sea-level projections, including vertical-land-movement rates as produced by NZ SeaRise (Naish et al. 2024). The red lines assume the same inter-seismic rate as previously published but include a static offset to account for any earthquake displacements, with the remaining lines including the change in vertical-land-movement rates projected out over the different time periods.

Much of the Kaikōura district, where there was the largest co- and post-seismic uplift from Kaikōura, has had a reduction in their relative sea-level rise projections. Most significant are points located west of Clarence River where the averaged earthquake uplift is almost 2 m. In these areas, even if the current uplift rates were to stop today and return to the ~1 mm/yr of inter-seismic subsidence, there would be a net decrease in the relative sea-level rise out beyond 2150 (Figure 4.2). In contrast, the area immediately south of Hundalee, where there has been co-seismic subsidence and decreasing uplift rates, there is a net increase in relative sea-level rise. Here, the total relative sea-level rise at 2050 based on the updated vertical land movement will occur ~14–40 years earlier than based on the inter-seismic rates (Figure 4.2).

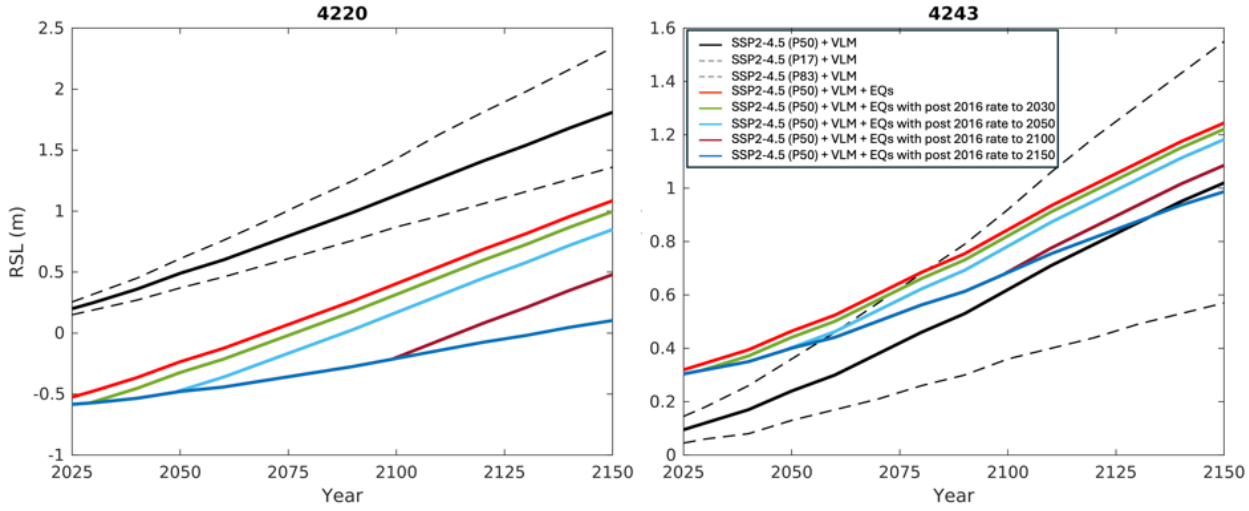

Figure 4.2 Re-projected vertical-land-movement estimates for points near Kaikōura and Hundalee (Figure 4.1) for the different scenarios discussed in the main text. The numbered titles reference the original NZ SeaRise identification numbers. Note that the offset between the NZ SeaRise (black) and updated projections are a result of the net uplift or subsidence caused by all of the earthquakes and the applied change in vertical-land-movement rate from 2016 to 2025.

Within the Christchurch urban area, the overall pattern of vertical land movement and associated relative sea-level rise estimates are largely consistent with those detailed in Hamling and Kearse (2023a). However, there is a general reduction in the estimated rates of subsidence compared with Hamling and Kearse (2023b). This is likely a result of the improved GNSS tie, addition of the descending data giving a more robust separation of the horizontal and vertical components of the deformation and a longer observation period. Although the rates are lower, the longer time series used here still shows elevated rates of subsidence around New Brighton Spit, resulting in up to 0.7 m of additional relative sea-level rise by 2150 compared with the NZ SeaRise projections (Naish et al. 2024). In the more likely case, where subsidence reverts close to its pre-earthquake rate in the next 10–30 years, there would be an additional ~0.3 m of relative sea-level rise (Figure 4.4). Higher rates of localised subsidence are also observed in Sumner and around Lyttleton Port, causing a net increase in the estimated relative sea-level rise compared with the NZ SeaRise projections.

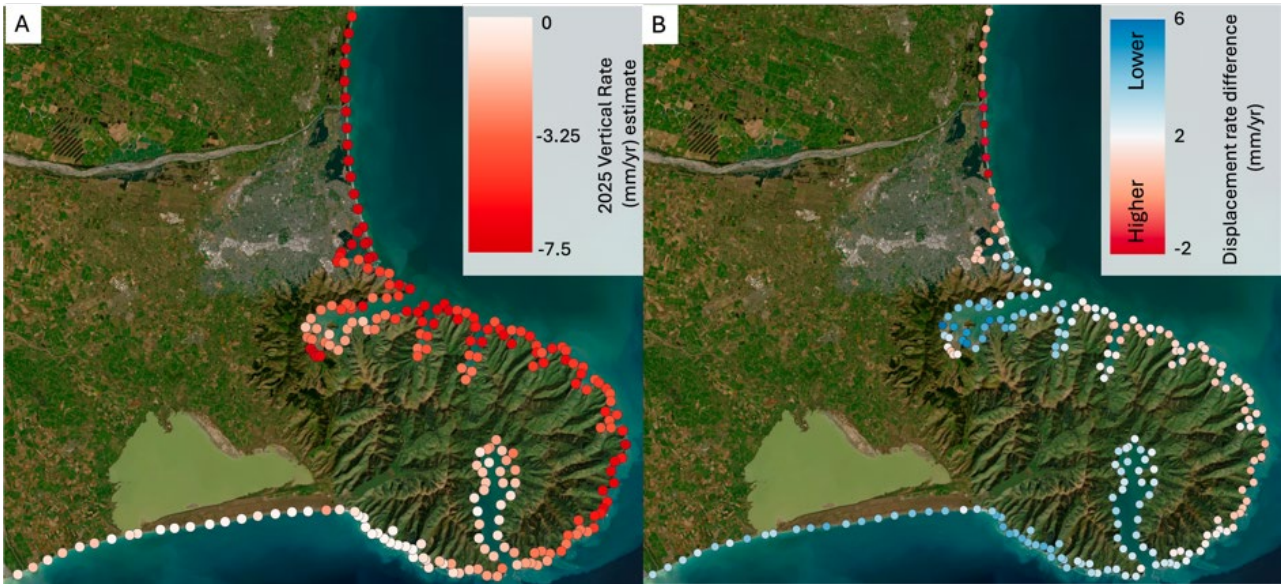

Figure 4.3 (A) Updated vertical land movement covering the same area as in Hamling and Kearse (2023b). (B) Difference in the estimated vertical-land-movement rates based on this analysis and Hamling and Kearse (2023b). Warm colours show areas where these rates are higher and cold colours where lower.

Around northern Banks Peninsula, from Adderly Head to Akaroa Head, there is ~3–4 mm/yr of estimated subsidence, slightly lower than the rates in Hamling and Kearse (2023b), which fixed these to an average regional subsidence of 4.6 mm/yr due to lack of InSAR coverage. The rate of subsidence decreases towards the southwest, where the co- and post-seismic influence of the earthquakes is minimal. Here, the re-estimated rates are generally consistent with the original NZ SeaRise inter-seismic estimates showing -2 to 0 mm/yr (Figures 4.1 and 4.4). However, given the improved data quality and GNSS tie, these new rates should provide an improved estimate to those on the NZ SeaRise portal and could be used until the new national relative sea-level rise / vertical land movement dataset is rolled out.

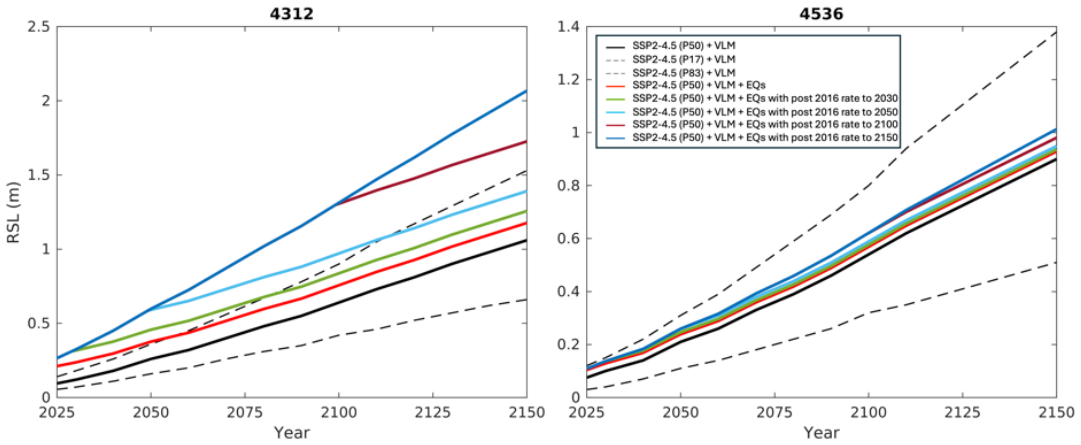

Figure 4.4 Re-projected vertical land movement estimates for points on New Brighton spit (left) and within the Ashburton district (right) for the different scenarios discussed in the main text. The numbered titles reference the original NZ SeaRise identification numbers. Note that the offset between the NZ SeaRise (black) and updated projections are a result of the net uplift or subsidence caused by all of the earthquakes and the applied change in vertical-land-movement rate from 2016 to 2025.

5.0 Conclusions

Based on this updated analysis, a combination of regional and local factors are contributing to the current estimates of vertical land movement. On the regional scale, post-seismic deformation in the vicinity and to the north of Kaikōura is dominated by continued uplift. Around Christchurch, regional subsidence continues at rates of ~4 mm/yr, with localised areas showing higher rates of subsidence frequently correlating to the underlying geology or recent construction. The largest post-seismic rates are observed across the New Brighton spit and into Southshore, where rates are approaching ~10 mm/yr. South of Banks Peninsula, the new vertical-land-movement rates estimated here are in good general agreement with the original NZ SeaRise vertical land movement and should provide an improved estimate to those on the NZ SeaRise portal. Although challenging to definitively put a timescale on how long some of the observed post-seismic vertical-land-movement rates will continue, under the scenario where the rates return to close to their inter-seismic value within the next 10–25 years, the majority of coastline's projected relative sea-level rise (to 2150) largely falls within the 17th to 83rd percentile values (66% 'likely' range) previously estimated through the NZ SeaRise programme. However, in areas with significant co- and post-seismic subsidence, the current relative sea level as of 2025 exceeds the NZ SeaRise projections.

Yours sincerely,

Ian Hamling
InSAR Scientist

6.0 References

Ansari H, De Zan F, Parizzi A. 2021. Study of systematic bias in measuring surface deformation with SAR interferometry. *IEEE Transactions on Geoscience and Remote Sensing*. 59(2):1285–1301. https://doi.org/10.1109/TGRS.2020.3003421

Beavan J, Motagh M, Fielding EJ, Donnelly N, Collett D. 2012. Fault slip models of the 2010–2011 Canterbury, New Zealand, earthquakes from geodetic data and observations of postseismic ground deformation. *New Zealand Journal of Geology and Geophysics*. 55(3):207–221. https://doi.org/10.1080/00288306.2012.697472

Blewitt G, Hammond WC, Kreemer C. 2018 Sep 24. Harnessing the GPS data explosion for interdisciplinary science. *Eos*; [accessed 2025 Apr]. https://doi.org/10.1029/2018EO104623

Diederichs A, Nissen EK, Lajoie LJ, Langridge RM, Malireddi SR, Clark KJ, Hamling IJ, Tagliasacchi A. 2019. Unusual kinematics of the Papatea fault (2016 Kaikōura earthquake) suggest anelastic rupture. *Science Advances*. 5(10):eaax5703. https://doi.org/10.1126/sciadv.aax5703

Fox-Kemper B, Hewitt HT, Xiao C, Aðalgeirsdóttir G, Drijfhout SS, Edwards TL, Golledge NR, Hemer M, Kopp RE, Krinner G, et al. 2021. Ocean, cryosphere and sea level change. In: Masson-Delmotte V, Zhai P, Pirani A, Connors SL, Péan C, Berger S, Caud N, Chen Y, Goldfarb L, Gomis MI, et al., editors. *Climate change 2021: the physical science basis – Working Group I contribution to the sixth assessment report of the Intergovernmental Panel on Climate Change*. Cambridge (GB): Cambridge University Press. p. 1211–1361. https://doi.org/10.1017/9781009157896.011

Garner GG, Hermans T, Kopp RE, Slangen ABA, Edwards TL, Levermann A, Nowikci S, Palmer MD, Smith C, Fox-Kemper B, et al. 2021. IPCC AR6 sea level projections. Version 20210809. Geneva (CH): CERN: European Organisation for Nuclear Research; [accessed 2025 Apr]. https://doi.org/10.5281/zenodo.5914709

Hamling IJ. 2020. A review of the 2016 Kaikōura earthquake: insights from the first 3 years. *Journal of the Royal Society of New Zealand*. 50(2):226–244. https://doi.org/10.1080/03036758.2019.1701048

Hamling IJ, Kearse J. 2023a. Inter-seismic, co-seismic and post-seismic rates of vertical land movement in the Christchurch district and implications for future changes in sea level. Lower Hutt (NZ): GNS Science. 19 p. Consultancy Report 2023/81. Prepared for Christchurch City Council; Environment Canterbury.

Hamling IJ, Kearse J. 2023b. Inter-seismic, co-seismic and post-seismic rates of vertical land movement in the Christchurch district and implications for future changes in sea level. Lower Hutt (NZ): GNS Science. Consultancy Report 2023/81. Prepared for Christchurch City Council; Environment Canterbury. Appendix 2, Addendum; 8 p.

Hamling IJ, Hreinsdóttir S, Clark K, Elliott J, Liang C, Fielding E, Litchfield N, Villamor P, Wallace L, Wright TJ, et al. 2017. Complex multifault rupture during the 2016 Mw 7.8 Kaikōura earthquake, New Zealand. *Science*. 356(6334):eaam7194. https://doi.org/10.1126/science.aam7194

Hamling IJ, Wright TJ, Hreinsdóttir S, Wallace LM. 2022. A snapshot of New Zealand's dynamic deformation field from Envisat InSAR and GNSS observations between 2003 and 2011. *Geophysical Research Letters*. 49(2):e2021GL096465. https://doi.org/10.1029/2021GL096465

Hughes MW, Quigley MC, van Ballegooy S, Deam BL, Bradley BA, Hart DE, Measures R. 2015. The sinking city: earthquakes increase flood hazard in Christchurch, New Zealand. *GSA Today*. 25(3):4–10. https://doi.org/10.1130/GSATG221A.1

Hussain E, Wright TJ, Walters RJ, Bekaert DPS, Lloyd R, Hooper A. 2018. Constant strain accumulation rate between major earthquakes on the North Anatolian Fault. *Nature Communications*. 9(1):1392. https://doi.org/10.1038/s41467-018-03739-2

Ingleby T, Wright TJ. 2017. Omori-like decay of postseismic velocities following continental earthquakes. *Geophysical Research Letters*. 44(7):3119–3130. https://doi.org/10.1002/2017GL072865

Kopp RE, Garner GG, Hermans THJ, Jha S, Kumar P, Reedy A, Slangen ABA, Turilli M, Edwards TL, Gregory JM, et al. 2023. The Framework for Assessing Changes To Sea-level (FACTS) v1.0-rc: a platform for characterizing parametric and structural uncertainty in future global, relative, and extreme sea-level change. *Geoscientific Model Development*. 16(24):7461–7489. https://doi.org/10.5194/gmd-16-7461-2023

Langridge RM, Rowland J, Villamor P, Mountjoy J, Townsend DB, Nissen E, Madugo C, Ries WF, Gasston C, Canva A, et al. 2018. Coseismic rupture and preliminary slip estimates for the Papatea Fault and its role in the 2016 Mw 7.8 Kaikōura, New Zealand, earthquake. *Bulletin of the Seismological Society of America*. 108(3B):1596–1622. https://doi.org/10.1785/0120170336

Naish T, Levy R, Hamling I, Hreinsdóttir S, Kumar P, Garner GG, Kopp RE, Golledge N, Bell R, Paulik R, et al. 2024. The significance of interseismic vertical land movement at convergent plate boundaries in probabilistic sea-level projections for AR6 scenarios: the New Zealand case. *Earth's Future*. 12(6):e2023EF004165. https://doi.org/10.1029/2023EF004165

Pearson C, Denys P. 2024. Christchurch City ground height monitoring – vertical land motion in eastern Christchurch. Christchurch (NZ): Environment Canterbury Regional Council.

Spaans K, Hooper A. 2016. InSAR processing for volcano monitoring and other near-real time applications. *Journal of Geophysical Research: Solid Earth*. 121(4):2947–2960. https://doi.org/10.1002/2015JB012752

Wallace LM, Hreinsdóttir S, Ellis S, Hamling I, D'Anastasio E, Denys P. 2018. Triggered slow slip and afterslip on the southern Hikurangi subduction zone Following the Kaikōura earthquake. *Geophysical Research Letters*. 45(10):4710–4718. https://doi.org/10.1002/2018GL077385

Wang H, Wright TJ. 2012. Satellite geodetic imaging reveals internal deformation of western Tibet. *Geophysical Research Letters*. 39(7):L07303. https://doi.org/10.1029/2012GL051222

Watson AR, Elliott JR, Lazecký M, Maghsoudi Y, McGrath JD, Walters RJ. 2024. An InSAR-GNSS velocity field for Iran. *Geophysical Research Letters*. 51(10):e2024GL108440. https://doi.org/10.1029/2024GL108440

APPENDIX 1 Additional Files

Filename	Description	Report Section
052A_NZMarlborough_001612_GNS_hre_Hurunui_00.shp *052A_NZMarlborough_001612_GNS_hre_Hurunui_01.shp* *052A_NZMarlborough_001612_GNS_hre_Hurunui_02.shp* *052A_NZMarlborough_001612_GNS_hre_Hurunui_03.shp* *052A_NZMarlborough_001612_GNS_hre_Hurunui_04.shp* *052A_NZMarlborough_001612_GNS_hre_Hurunui.shp* *052A_NZMarlborough_001612_GNS_hre_Kaik_00.shp* *052A_NZMarlborough_001612_GNS_hre_Kaik_01.shp* *052A_NZMarlborough_001612_GNS_hre_Kaik.shp* *073D_13389_NZ_GNS_hre_Ashburton_00.shp* *073D_13389_NZ_GNS_hre_CD_00.shp* *073D_13389_NZ_GNS_hre_CD_01.shp* *073D_13389_NZ_GNS_hre_CD_02.shp* *073D_13389_NZ_GNS_hre_CD_03.shp* *073D_13389_NZ_GNS_hre_CD_04.shp* *073D_13389_NZ_GNS_hre_CD_05.shp* *073D_13389_NZ_GNS_hre_CD_06.shp* *073D_13389_NZ_GNS_hre_Hurunui_00.shp* *073D_13389_NZ_GNS_hre_Hurunui_01.shp* *073D_13389_NZ_GNS_hre_Selwyn_00.shp* *073D_13389_NZ_GNS_hre_Selwyn_01.shp* *073D_13389_NZ_GNS_hre_Timuru_00.shp* *073D_13389_NZ_GNS_hre_Waimakariri_00.shp* *073D_13389_NZ_GNS_hre_Waimakariri_01.shp* *073D_NZMarlborough_101311_GNS_hre_Hurunui_00.shp* *073D_NZMarlborough_101311_GNS_hre_Kaik_00.shp* *125A_13313_NZ_GNS_hre_Ashburton_00.shp* *125A_13313_NZ_GNS_hre_Ashburton_01.shp* *125A_13313_NZ_GNS_hre_CD_00.shp* *125A_13313_NZ_GNS_hre_CD_01.shp* *125A_13313_NZ_GNS_hre_CD_02.shp* *125A_13313_NZ_GNS_hre_CD_03.shp* *125A_13313_NZ_GNS_hre_CD_04.shp* *125A_13313_NZ_GNS_hre_CD_05.shp* *125A_13313_NZ_GNS_hre_CD_06.shp* *125A_13313_NZ_GNS_hre_CD_07.shp* *125A_13313_NZ_GNS_hre_Hurunui_00.shp* *125A_13313_NZ_GNS_hre_Hurunui_01.shp* *125A_13313_NZ_GNS_hre_Selwyn_00.shp* *125A_13313_NZ_GNS_hre_Selwyn_01.shp* *125A_13313_NZ_GNS_hre_Timuru_00.shp* *125A_13313_NZ_GNS_hre_Waimakariri_00.shp* *125A_13313_NZ_GNS_hre_Waimakariri_01.shp* *146D_13386_NZ_GNS_hre_Timuru_00.shp*	Shapefiles containing the original LOS displacement time series for each of the satellite passes used in the analysis. Files are split into the different districts (e.g. Hurunui, Kaikōura). To manage the size of the files, these are also split into multiple files indicated by the number at the end of the filename (00, 01, etc.). As these files contain the LOS displacement values, their time-series values are a combination of the horizontal and vertical components of ground movement. Despite the measurement being in the LOS direction, the temporal evolution of individual points will give an indication of the stability (or not) of the point and show any seasonality to its movement. In addition to the time series, each file contains an estimate of the linear LOS displacement rate, the RMSE of the point and the average coherence of the point. The latter two metrics provide an estimate of the overall stability of the pixel, where a low RMSE and high coherence indicate a more stable reflector.	Section 3, Figure 3.1

Filename	Description	Report Section
Full_vertical_CCC-ECAN.txt	Best-fitting vertical-displacement rate and error estimates after tying off the InSAR and GNSS datasets. Vertical estimates are provided on a 50 m grid within the CCC district and 100 m elsewhere. The derived vertical estimates come from the merging of the interpolated long-wavelength and InSAR LOS datasets following the methodology described in Section 3.	Section 3, Figure 3.3
GNSS_vertical_only.txt	Best-fitting vertical-displacement rate interpolated from the vertical GNSS data, providing an estimate of the long-wavelength vertical motion and background vertical land movement. Note that, while the values at or near to GNSS sites are well resolved, uncertainties away from the sites will increase, as these are estimated from the interpolation of the sparser GNSS network.	Section 3, Figure 3.2
Vertical_CCC-ECAN-2km.txt	Binned vertical rates at 2 km intervals matching with the NZ SeaRise coastal strip. The file contains the site identification numbers, longitude, latitude, vertical-land-movement rates and errors. The file also has the number of data points used to estimate the vertical land movement for each of the 2 km samples and the average distance of the points to the sample location.	Section 4
All_EQ_def.txt	File containing the predicted vertical co-seismic displacements based on the slip models described in Section 2. All of the displacements are in metres.	Section 2, Figure 2.1
Vertical_interp.tif	GeoTIFF of interpolated vertical rates. Values are based on a linear interpolation using a Delauney triangulation of the sample points, whereby the interpolated value is the weighted sum of the values of the three vertices of the enclosing triangular element. Other interpolation approaches, such as nearest neighbour, produce similar results but were found to be less smooth.	N/A
VLM_projections_SSP2-4.5.txt	Re-projections of relative sea-level rise based on the methods described in the main body of the report, including the different post-seismic vertical-land-movement changes at different times.	Section 4